

# Preferential flow control in heterogeneous porous media by concentration-manipulated rheology of microgel particle suspension

Wenhai Lei<sup>a</sup>, Qiangqiang Li<sup>a</sup>, Hai-En Yang<sup>b</sup>, Tian-Jiang Wu<sup>b</sup>, Jiong Wei<sup>a</sup>, Moran Wang<sup>a,\*</sup>

<sup>a</sup> Department of Engineering Mechanics, Tsinghua University, Beijing, 100084, China

<sup>b</sup> Changqing Oilfield, PetroChina, Xi'an, Shaanxi, 710018, China

## ARTICLE INFO

### Keywords:

Preferential flow  
Microgel particle suspension  
Rheology  
Porous media

## ABSTRACT

Preferential flow is commonly encountered but decreases the efficiency of multiphase displacement in most industrial processes. Microgel particle suspensions with polymer/colloid duality are a potential candidate to overcome such nonuniform flow. In this study, a novel mechanism of preferential flow control in heterogeneous porous media by concentration-manipulated rheology of microgel particle suspension was proposed, which is strongly supported by microfluidic experiments and pore-scale simulations. By varying the injection concentration, displacement processes were identified to three transport modes: the channeling mode at a low injection concentration, the synchronous mode at an intermediate injection concentration, and the fluctuation mode at a high injection concentration. Concentration-manipulated rheology and nonuniform particle concentration distribution in different layers make it possible to realize uniform flow in heterogeneous porous media. It was demonstrated that the multiphase processes at low/intermediate injection concentrations are dominated by two-phase flow with particle advection-diffusion in the invading phase but that at high injection concentrations disobeys this model due to local particle rapid enrichment by particles lagging behind the displacing fluid. During the displacement process, an intermediate injection concentration always exhibits the optimal synchronous displacement by self-adaptive concentration manipulation in different layers. However, concentration manipulation at low injection concentrations was too weak to suppress preferential flow, and a high injection concentration was sensitive enough to alternate preferential flow pathways frequently, which will lead to oleic ganglia being trapped. These findings deepen the understanding of microgel particle suspension dynamics in heterogeneous porous media and shed unique insights for their applications, such as enhanced oil recovery and CO<sub>2</sub> sequestration.

## 1. Introduction

A preferential flow pathway is naturally formed in heterogeneous porous media, where fluid prefers to travel through low-resistance pathways. Such an uneven flow pattern has attracted much attention due to its importance in diverse natural and engineering processes, e.g., drug delivery in vascular networks (Sackmann et al., 2014), enhanced oil recovery (EOR) (Blunt, 2017), water infiltration through soils (Cue-to-Felgueroso and Juanes, 2008), and geological carbon sequestration (Huppert and Neufeld, 2014). However, the heterogeneity of microstructures and hydraulic properties that widely exists in geological formations poses great technical challenges for the efficiency and economy of multiphase displacement. For instance, in reservoir engineering, injection fluid skirts around the low permeable region so that a

considerable amount of the remaining oil is trapped in the unswept formation (Datta et al., 2014). These multiphase processes are critically affected not only by the inherent architecture of porous solids (Le Goc et al., 2010; Siena et al., 2019) but also by fluid properties (Levaché and Bartolo, 2014; Xie et al., 2020). To optimize multiphase flooding operations and thus improve displacement efficiency, it is essential to understand and suppress preferential flow in heterogeneous porous media.

Extensive studies have been devoted to revealing the preferential flow formation mechanism from a large scale (Arshadi et al., 2018; Khan et al., 2016; Moreno and Tsang, 1994; Watanabe et al., 2009) down to the pore scale (Cieplak and Robbins, 1988, 1990; Holtzman and Segre, 2015; Hu et al., 2019; Lenormand et al., 1983; Rabbani et al., 2018). In a pioneering pore-scale work, Lenormand et al. (1983) experimentally studied a drainage process in a micromodel and demonstrated that the

\* Corresponding author.

E-mail address: [mrwang@tsinghua.edu.cn](mailto:mrwang@tsinghua.edu.cn) (M. Wang).

<https://doi.org/10.1016/j.petrol.2022.110275>

Received 8 September 2021; Received in revised form 25 November 2021; Accepted 9 February 2022

Available online 12 February 2022

0920-4105/© 2022 Elsevier B.V. All rights reserved.

competition between viscous and capillary forces controls the instability of the fluid-fluid interface, which results in macroscopic patterns ranging from capillary fingering to viscous fingering to compact displacement. Later, the competing relation became more complicated by considering the effects of wettability (Holtzman and Segre, 2015; Hu et al., 2019; Zhao et al., 2016) and pore structure (Rabbani et al., 2018; Suo et al., 2020; Wang et al., 2019). Holtzman and Segre (2015) conducted pore-scale simulations and found that a decrease in the contact angle stabilized the invasion process, but a high flow rate promoted preferential flow formation. Rabbani et al. (2018) combined microfluidic experiments and pore-scale simulations to demonstrate that the gradient pore size effect can stabilize the displacement process and suppress preferential flow.

Unlike the interfacial instability-induced preferential flow in homogeneous or single-permeability systems, preferential flow formation in heterogeneous porous media with permeability contrast is more popular but complex in natural geological formations. Injection of a viscous fluid such as continuous polymer solution may stabilize the fluid-fluid interface, but merely increasing viscosity will not further mediate the flow rate difference in unfavorable heterogeneous structures (Browne et al., 2020; Xie et al., 2018). Therefore, foam, as a typical dispersed system, seems to be an alternative method for preferential flow control. Ma et al. (2012) demonstrated that foam could divert invading flow from high-permeability to low-permeability regions in a dual-permeability micromodel. Conn et al. (2014) further presented the novel oil displacement mechanisms of foam as a nonhomogeneous gas/liquid dispersion in a dual-permeability micromodel. However, foam application in reservoir engineering is hindered by difficulties in production, invalidation at high temperature/salinity, and high costs (Lai et al., 2018; Wang et al., 2021). Considering that dispersed polymers can overcome the above disadvantages, Xie et al. (2021) performed dispersed polymer system transport in heterogeneous porous media by pore-scale numerical simulation and proved that such a dispersed phase could realize better conformance control than simply increasing the viscosity by the continuous phase. Inspired by this research, the combination of the non-Newtonian and dispersion features was adopted in this study. Microgel particle suspensions with polymer/colloid duality are a potential candidate to overcome preferential flow and provide better conformance control under various harsh conditions (Lei et al., 2019, 2020; Monteillet et al., 2014). In addition, some advantages have also been reported: deformable particles may increase the stability of emulsions (Gong et al., 2017; Monteillet et al., 2014; Style et al., 2015), and micro- and nanoscale particles can migrate into deep formations to alter wettability (Gong et al., 2018; Liu et al., 2019).

The impact of microgel particle suspensions on the multiphase flow process has been studied in extensive laboratory experiments, and its significance and excellent capability have been ascribed mainly to the plugging effect (Abdulbaki et al., 2014; Imqam et al., 2018; Li et al., 2020; Zhang and Bai, 2011). In core-scale studies, researchers have found that microgel particle suspensions can largely reduce rock permeability and generate sharp pressure pulses in the position where the microgel particle suspension plugs and remigrates (Imqam et al., 2018; Smith et al., 2000; Zhao et al., 2018). In pore-scale studies, different particle transport modes have been investigated and classified as adsorption mode, direct pass mode, deform-pass mode, and deform/bridge plugging mode (Yao et al., 2014; Zhao et al., 2013). Quantitatively, the size matching rule was proposed based on the plugging effect in which the optimal matching ratio between the particles and pores commonly ranged from 4–0.5 (Bai et al., 2007; Chen et al., 2020; Yao et al., 2013; Yuan et al., 2019). However, there are still many different results showing that smaller particles can also be effective. For example, the optimal matching ratios are 0.5–0.33 (Zhao et al., 2013), 0.21–0.29 (Dai et al., 2017), 0.33–0.14 (Abrams, 1977; Barkman and Davidson, 1972), and less than 1/10 (Pritchett et al., 2003). Obviously, the picky blocking effect is not the only mechanism for the impact of microgel particle suspension on multiphase flow; in particular, it is

still effective using a small particle size with a minimal matching ratio. An incomplete understanding of the underlying physics of microgel particle suspension transport in porous media still limits the robust application of microgel particle suspensions (Imqam et al., 2018; Zhao et al., 2018).

In this study, the goal was to understand and control preferential flow in heterogeneous porous media using a microgel particle suspension with polymer/colloid duality and to elucidate how non-Newtonian features of fluid and particle advection-diffusion properties impact the multiphase flow pattern. It remains a great challenge to reveal the impact of microgel particle suspensions on the multiphase displacement mechanism because of the complex mechanical properties of micro-particles and suspensions, the visualization and quantification of microflow and microparticles, and multiphysical phenomena with particle diffusion and multiphase flow. Although much literature has documented the study of the nonlinear dynamics of miscible flow displacements by coupling the flow field and advection-diffusion process, such as Newtonian or non-Newtonian fluids (Shokri et al., 2017; Tan and Homsy, 1988), homogeneous or heterogeneous media (Shahnazari et al., 2018), and concentration-dependent diffusion coefficients (Yuan et al., 2018), the immiscible multiphase displacement dynamics of microgel particle suspensions with concentration manipulated rheology in a heterogeneous porous system are still not well understood.

In this work, microfluidic experiments and numerical simulations were combined to study the preferential flow suppression mechanism of microgel particle suspensions. The polymer/colloid duality of the microgel particle suspension was characterized and concluded to be concentration-dependent rheology. Heterogeneous microfluidic structures were fabricated with permeability contrast and the preferential flow formation and suppression process was imaged. A pore-scale numerical simulation coupled with non-Newtonian Navier-Stokes equations, an advection-diffusion equation, and the Cahn-Hilliard equation was used to reproduce the main displacement process. Based on experimental observations and numerical simulations, it was determined that different concentrations were manipulating preferential flow behaviors from macroscopic patterns to pore-scale mechanisms. Finally, new mechanisms of microgel particle suspension for preferential flow control were determined, which may lead to efficient oil/gas recovery and CO<sub>2</sub> storage.

## 2. Microgel synthesis and characterization

### 2.1. Materials and microgel particle synthesis

The microgel particle suspensions used in this study were prepared by diluting the stock microgel particle suspension with deionized water to achieve the desired injection concentration. The stock microgel particle suspension was synthesized by the following materials: acrylamide (20%, purity above 98.5%), water-soluble anionic monomer (10%, acrylic acid & sodium acrylate), third monomer (5%, acrylate), dispersion stabilizer (15%, Span 60 & Tween 60), solvent 1 (40%, mineral oil), solvent 2 (1%, xylenes), and deionized water (9%). All chemical reagents were purchased from Shanghai Macklin Biochemical Co., Ltd. (China) without any further purification. The inverse suspension polymerization method was carried out to make micron-grade microgel particles in the laboratory of Technical Institute of Physics and Chemistry, Chinese Academy of Sciences. During the synthesis process, the continuous phase was the oleic phase, the dispersed phase was the aqueous phase, and the monomer aqueous solution was divided into several reactive microdomains by surfactants to prepare microgel particles. To observe the particles more clearly in the visual experiments, the surface of all the particles was modified with fluorescence.

### 2.2. Characterization methods

A cryo-scanning electron microscope (cryo-SEM, Helios NanoLab

G3UC, USA) equipped with a Quorum PP3010T cryo-system was used to observe the in situ morphology of the microgel particles. The structures of microgel particles in the oleic stock suspension in the original state and in the diluted aqueous suspension in the application state were compared. Correspondingly, the particle size distribution of microgel particle suspensions with different concentrations in the oleic phase and aqueous phase was measured by dynamic light scattering (DLS) via a

Malvern Zetasizer Pro and Mastersizer 3000 E Hydro (Malvern Instruments, U.K.) using refractive indices of the oleic phase, polymer microsphere and aqueous phase of 1.41, 1.50 and 1.33, respectively. Rheological characterization was performed using a rheometer (Hakke Mars III, Thermo Fisher Scientific, USA) equipped with a stainless steel upper cone plate as a clamping fixture (diameter 60.006 mm, cone angle  $0.989^\circ$ , Model C60/1° TiL). The viscosity was measured under state

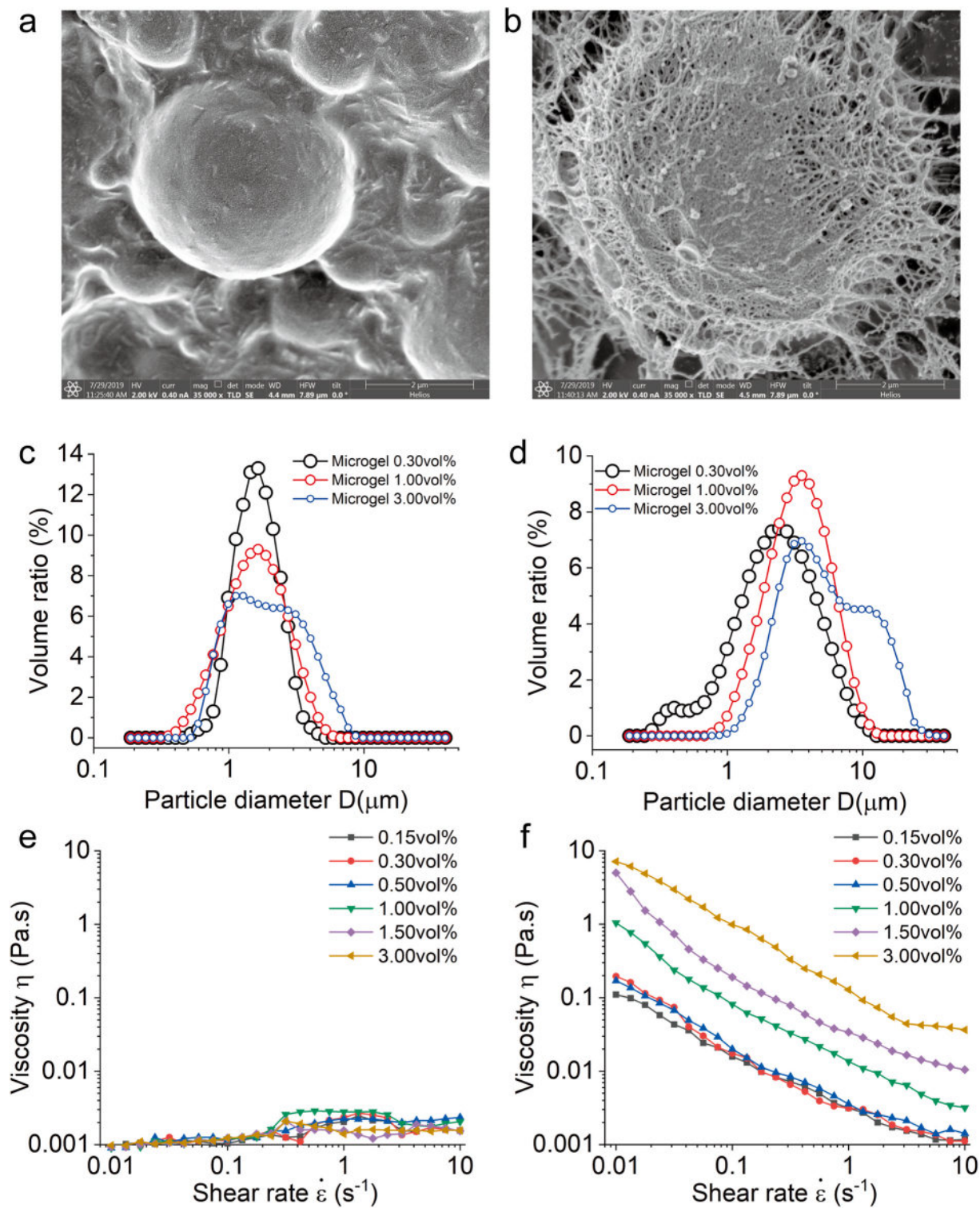


**Fig. 1.** Characterization of microgel particle suspension diluted in (a,c,e) oil and (b,d,f) water. Cryo-SEM micrograph of the particle structure diluted in (a) oil and (b) water. Microgel particle size distribution with different concentrations diluted in (c) oil and (d) water. Viscosity versus the shear rate of the microgel particle suspension with different concentrations in (e) oil and (f) water.

shearing modes, where the shearing rate ranged from 0.01 to 10 s<sup>-1</sup> at a constant of 20 °C.

### 2.3. Characterization results

Fig. 1a and b shows the in situ morphology of the microgel particles in the oleic stock suspension and the diluted aqueous suspension, respectively. When it is diluted in water, contrary to its smooth surface in the original oleic suspension, the hydrophilic polymer chains on the surface of the particles open up quickly, and a complex spherical network structure is formed (see Fig. 1b). Although such morphological differences have almost no effect on the particle size distribution (see Fig. 1c and d), the rheological properties of the microgel particle suspension are largely affected (see Fig. 1e and f).

The particle size distributions of the microgel particle suspensions with desired bulk concentrations of 0.3 vol%, 1.0 vol% and 3.0 vol% diluted in the oleic phase and the aqueous phase are shown in Fig. 1c and d, respectively. To avoid the influence of oil droplets in the suspension, the diluted microgel particle suspensions were centrifuged at 2000 r/s for 4 min to remove the upper layer of the oil phase, and then the lower part of the microsphere suspension was dispersed uniformly by ultrasonication at 80 W for 10 min. The characteristic particle sizes (D<sub>50</sub>, the particle size of the 50% cumulative probability) diluted in the oleic phase are 1.45 μm, 1.47 μm, and 1.65 μm, and those diluted in the aqueous phase were 2.13 μm, 3.12 μm, and 4.58 μm.

In the oleic phase, the concentration of particles had little effect on the viscosity as a Newtonian fluid due to good dispersibility, and all polymer chains are locked inside the particles (Fig. 1e). However, in the aqueous phase, the microgel particles present the dual characteristics of colloids and polymers with concentration-dependent non-Newtonian characteristics due to the hydrophilic polymer chains on the surface of the particles and the networked structure (Fig. 1f).

The non-Newtonian characteristic of microgel particle suspension presented the features of a power-law fluid, and the fitting relationship between viscosity  $\eta$ , shear rate  $\dot{\epsilon}$  and concentration  $c$  is  $\eta_m = (10^{0.11c^2+0.62c-2.56})\dot{\epsilon}^{-0.786}$ , which will be inputted into non-Newtonian Navier-Stokes equations of the simulation model. Other parameters were also measured for the experimental and simulation analyses, as shown in Table 1. The dynamic viscosity of other fluids will be entered into Newtonian Navier-Stokes equations. Interface tension and contact angle will be used in the Cahn-Hilliard equation for fluid-fluid and fluid-solid interactions. The diffusion coefficient was related to the parameters of the advection-diffusion equation. The concentration of microgel particle suspension used in this study only has a strong impact on non-Newtonian properties (effective viscosity) but a weak impact on other factors (e.g., particle size, wettability, interfacial tension, and density).

## 3. Microfluidic experiments and numerical simulation

### 3.1. Microfluidic platform and bipermiability micromodels

Fig. 2a shows the micromodel microscopy system, which was an improvement on a previously designed system (Lei et al., 2020; Xie et al., 2021). It consists of a fluorescence microscope (SMZ18, Nikon, Japan) with a high-speed camera (DS-Ri2, Nikon, Japan), a microfluidic pressure controller (MFCS-8C, Fluigent, France) connected to three fluid reservoirs, and a flow information monitoring system with a flow rate sensor (FRP, Fluigent, France) and a pressure transducer (P61, Validyne, USA).

The micromodels used in this study were fabricated at Tsinghua Nanofabrication Technology Center. First, the porous structure of the micromodel with an artificial bipermiability porous structure was designed to purify the preferential flow formation and suppression process, as shown in Fig. 2b. Both layers were composed of cylindrical pillars with different radii aligned, and they had the same porosity

**Table 1**

The key parameters of the experiments and simulation analysis.

Property name	Property symbol	Value	Data sources	
Density of water	$\rho_w$	995 kg m <sup>-3</sup>	PubChem <sup>a</sup>	
Density of oil	$\rho_o$	725.5 kg m <sup>-3</sup>	PubChem <sup>a</sup>	
Density of MGPS <sup>b</sup>	at 0.3 vol %	$\rho_{mL}$	965 kg m <sup>-3</sup>	Experimental data
	at 1.0 vol %	$\rho_{mM}$	932 kg m <sup>-3</sup>	Experimental data
	at 3.0 vol %	$\rho_{mH}$	920 kg m <sup>-3</sup>	Experimental data
Dynamic viscosity	of water	$\eta_w$	0.8949 mPa·s	PubChem <sup>a</sup>
	of oil	$\eta_o$	0.838 mPa·s	PubChem <sup>a</sup>
Interface tension	of oil and water	$\gamma_{o-w}$	48.50 mN m <sup>-1</sup>	Experimental data <sup>c</sup>
	of oil and MGPS at 0.3 vol%	$\gamma_{o-mL}$	8.12 mN m <sup>-1</sup>	Experimental data <sup>c</sup>
	of oil and MGPS at 1.0 vol%	$\gamma_{o-mM}$	8.06 mN m <sup>-1</sup>	Experimental data <sup>c</sup>
	of oil and MGPS at 3.0 vol%	$\gamma_{o-mH}$	7.75 mN m <sup>-1</sup>	Experimental data <sup>c</sup>
Contact angle on solid grains	for oil and water	$\theta_{o-w}$	87°	Experimental data <sup>c</sup>
	for oil and MGPS at 0.3 vol%	$\theta_{o-mL}$	82°	Experimental data <sup>c</sup>
	for oil and MGPS at 1.0 vol%	$\theta_{o-mM}$	85°	Experimental data <sup>c</sup>
	for oil and MGPS at 3.0 vol%	$\theta_{o-mH}$	83°	Experimental data <sup>c</sup>
Diffusion coefficient	$D$	$1.40 \times 10^{-13} \sim 1.40 \times 10^{-16} \text{ m}^2\text{s}^{-1}$	Calculated by Stokes-Einstein relation <sup>d</sup>	

<sup>a</sup> The standard parameters of common chemicals come from PubChem (<http://pubchem.ncbi.nlm.nih.gov/>).

<sup>b</sup> MGPS is the abbreviation of microgel particle suspension.

<sup>c</sup> The interfacial tension  $\gamma$  and contact angle  $\theta$  were measured in our laboratory with a Drop Shape Analyzer (DSA25, Krüss) instrument based on the pendant drop and Young-Laplace fitting methods by placing an aqueous drop on the silicon wafer submerged in a decane-filled reservoir, respectively. The values over 4 h were selected as stable contact angle values to represent the system wettability.

<sup>d</sup> The Stokes-Einstein relation was used to calculate the diffusion coefficient  $D = \frac{kT}{6\pi r\eta}$ , where Boltzmann constant  $k = 1.38 \times 10^{-23}$ , temperature  $T = 298.15\text{K}$ , characteristic particle radius  $r = 1.56\mu\text{m}$ , and aqueous fluid viscosity  $\eta = 10^{-3} \sim 1$ , according to Fig. 1.

(45.45%); the total pore volume (PV) was 1.31 μL, and detailed information is shown in Fig. 2c. Notably, the smallest pore size of the micromodel was ten times larger than the microgel particle size described in Section 2. The permeability ratio of higher and lower permeable layers was estimated at 16:9 with the hydraulic radii of the pore throats,  $\frac{k_{\text{high}}}{k_{\text{low}}} = \left(\frac{R_{\text{high}}}{R_{\text{low}}}\right)^2 = \left(\frac{120 \times 60 / 360}{60^2 / 240}\right)^2 = \frac{16}{9}$ . Based on the obtained

structure, these micromodels were then fabricated on silicon via microfabrication techniques (Chomsurin and Werth, 2003; Grate et al., 2013), including standard photolithography and inductively coupled plasma-deep reactive ion etching (ICP-DRIE). The pattern silicon wafer was then anodically bonded to the Pyrex glass wafer (Schott, German) and diced to form a micromodel. Finally, to obtain an equal neutral-wet condition on all surfaces within the micromodel, the micromodel was

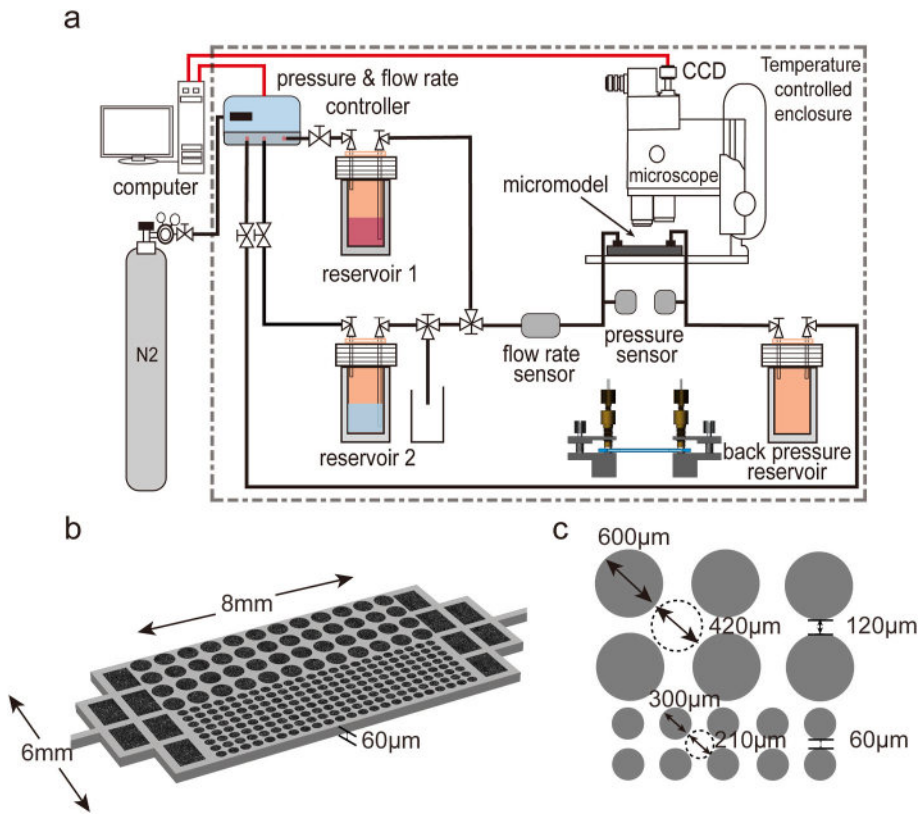


**Fig. 2.** Microfluidic platform and bipermiability micromodel. (a) Schematic diagram of our experimental setup. The red color in reservoir 1 is oil as the defending phase, and the blue color in reservoir 2 is the microgel particle suspension or water as the invading phase. (b) Dimensions of heterogeneous porous media composed of 232 discoid silica grains. (c) The micromodel pattern, with diameters  $D_H = 600 \mu\text{m}$  and  $D_L = 300 \mu\text{m}$  and widths  $d_H = 120 \mu\text{m}$  and  $d_L = 60 \mu\text{m}$ . The depth of pore throat was  $60 \mu\text{m}$ . (For interpretation of the references to color in this figure legend, the reader is referred to the Web version of this article.)

moderately modified by dichlorodimethylsilane to adjust its wettability to neutral-wet conditions.

### 3.2. Experiment procedure and image analysis

Prior to experiments, the micromodels were cleaned by 50 PV standard cleaning solution SC-1 (70 vol% deionized water, 15 vol% ammonium hydroxide, 15 vol% hydrogen peroxide) and 50 PV deionized water sequentially (Grate et al., 2013). Then, the micromodel was dried by  $\text{N}_2$  (5 bar) and vacuum treated for 12 h sequentially. The cleaned micromodel was assembled by a holder, and the experiments were conducted at normal temperature and pressure. A constant flow rate  $Q = 1 \mu\text{L min}^{-1}$  was chosen as the fluid injection flow rate for all experiments (the capillary number was  $1.75 \times 10^{-6}$ ), which corresponds to the real reservoir conditions, and its saturation will not vary significantly at such capillary numbers (Blunt, 2017; Datta et al., 2014). Any micromodels were reused to avoid the possibility of pore pollution. Then, the fluorescent dyed oil (100 ppm Nile red in decane) in reservoir 1 was injected until all pores of the micromodel were filled (Fig. 2a). When the pressure difference of the microchip as close to zero, the switch changed to Reservoir 2 (the invading fluid) to start the displacement experiments. Reservoir 3 was used as a waste liquid pool and to keep the constant back pressure (1 psi gas pressure).

Image processing was performed by the Image Processing Toolbox of MATLAB and involved making binary, filtering, subtracting pictures at different times, and removing noise of the generated picture to obtain the defending phase distribution. Then, the invading phase can be obtained by subtracting the binarized picture of the defending phase at different times from the initial binarized picture. Finally, the phase distribution and saturation of the invading and defending phases can be identified and calculated.

### 3.3. Pore-scale simulation method

Considering the difficulty of observing the velocity/pressure change in the flow field and particle concentration evolution in microfluidic experiments, a powerful numerical simulation for multiphase flow in porous media is an important tool to comprehensively study this problem. Based on the above characterization, coupled non-Newtonian Navier–Stokes equations, advection-diffusion equations, and Cahn–Hilliard equations were solved using a finite element method by COMSOL Multiphysics 5.5 to analyze the transport behaviors. In view of the approximations physics to two-dimensional (2D) simulations (Ferrari et al., 2015), the lack of complex 3D effects, and the expensive computation in 3D simulation, a series of 2D immiscible displacement simulations were performed in this paper.

The governing equations of immiscible displacement in porous media for this problem were described by the equations for the conservation of mass, the conservation of momentum in the form of the Navier–Stokes equations, and the advection-diffusion equation at the continuum scale as follows:

$$\rho \nabla \cdot \mathbf{u} = 0 \quad (1)$$

$$\rho \partial_t \mathbf{u} + \rho (\mathbf{u} \cdot \nabla) \mathbf{u} = -\nabla \cdot \mathbf{p} \mathbf{I} + \nabla \cdot \boldsymbol{\sigma} + \mathbf{F}_\gamma \quad (2)$$

$$\partial_t c + \mathbf{u} \cdot \nabla c = \nabla \cdot (D \nabla c) \quad (3)$$

where  $\rho$  is the fluid density,  $\mathbf{u}$  is the velocity vector,  $p$  is the pressure,  $\mathbf{I}$  is the identity tensor,  $\boldsymbol{\sigma}$  is the Cauchy stress tensor,  $\mathbf{F}_\gamma$  is in charge of the interfacial tension  $\gamma$ ,  $c$  is the particle concentration, and  $D$  is the diffusion coefficient.

The constitutive equation for water and oil as a Newtonian fluid is

$$\nabla \cdot \boldsymbol{\sigma} = \eta_w \nabla^2 \mathbf{u} \quad (4a)$$

and for a microgel particle suspension as a non-Newtonian (power-law) fluid is

$$\boldsymbol{\sigma} = 2\eta_m \mathbf{S} = m\dot{\epsilon}^{n-1}(\nabla \mathbf{u} + (\nabla \mathbf{u})^T) \quad (4b-1)$$

$$\dot{\epsilon} = \max\left(\sqrt{2\mathbf{S}:\mathbf{S}}, \dot{\epsilon}_{\min}\right), \mathbf{S} = \frac{1}{2}(\nabla \mathbf{u} + (\nabla \mathbf{u})^T) \quad (4b-2)$$

where  $\eta$  is the dynamic viscosity, the shear rate  $\dot{\epsilon}$  is calculated by  $\dot{\epsilon} = \sqrt{2\mathbf{S}:\mathbf{S}}$  with the shear rate tensor  $\mathbf{S}$ , and a low shear rate limit  $\dot{\epsilon}_{\min} = 0.01 \text{ s}^{-1}$  is used to avoid ultralow shear rate-induced ultrahigh shear stress according to the experimental data range. As shown in Section 2 about power-law fluid characterization,  $\eta_m = m\dot{\epsilon}^{n-1}$ ,  $m = 10^{0.11c^2+0.63c-2.59}$ ,  $n = 0.214$ .

In regard to multiphase flow, an additional equation is required to capture the interface evolution (Xie et al., 2016). The Cahn-Hilliard equation is the governing equation of the phase-field method (Cahn, 1959; Cahn and Hilliard, 1958, 1959), which stands out in its treatment of the interface as a physically diffuse thin layer by spreading the interfacial force over a volume (Yue et al., 2004, 2006). The general form is expressed as

$$\partial_t \varphi + \mathbf{u} \cdot \nabla \varphi = M \nabla^2 G \quad (5)$$

where  $\varphi$  is the order parameter,  $M$  is the mobility that controls the diffusion rate of the interface,  $G = \lambda \left[ -\nabla^2 \varphi + \frac{\varphi(\varphi^2-1)}{\epsilon^2} \right] = \frac{\lambda}{\epsilon^2} \psi$  is the chemical potential,  $\lambda$  is the mixing energy density with the dimension of

force, and  $\epsilon$  is a capillary width that scales with the thickness of the diffuse interface. As  $\epsilon \rightarrow 0$ , the ratio  $\lambda/\epsilon$  produces the interfacial tension  $\gamma$  in the classical sense  $\gamma = \frac{2\sqrt{2}}{3} \frac{\lambda}{\epsilon}$ . The interfacial tension in the Navier–Stokes equations as a volume force  $F_\gamma = G \nabla \varphi$  and the contact angle  $\theta$  in the phase-field method can be described by  $\mathbf{n} \cdot \epsilon^2 \nabla \varphi = \epsilon^2 \cos(\theta) |\nabla \varphi|$  (Yue et al., 2004).

Microgel particles cannot move from the aqueous phase to the nonaqueous phase, and the fluid–fluid interface is impenetrable for microgel particles; the fluid–fluid boundary condition is:

$$\nabla c \cdot \nabla \varphi = 0 \quad (6)$$

The structure, fluid properties, and flow conditions in the simulations are the same as those in the corresponding microfluidic experiments. The injection flow rate was set as  $v = Q/A = 1.1 \times 10^{-3} \text{ m/s}$ , and the flow rate was  $Q = 1 \mu\text{L min}^{-1}$ . Due to the separation and hydrodynamic filtration caused by micron particle transport in the long injection tube before the displacement process (Lenshof and Laurell, 2010; Yamada and Seki, 2005), 0.08 PV ( $t = 10 \text{ s}$ ) water was injected first as a buffer layer, and then the injection of microgel particles was started in our simulation. Note that wettability could also affect the flow preference (Gu et al., 2021), which can be ignored reasonably in our microfluidic experiments due to the neutral-wet condition.

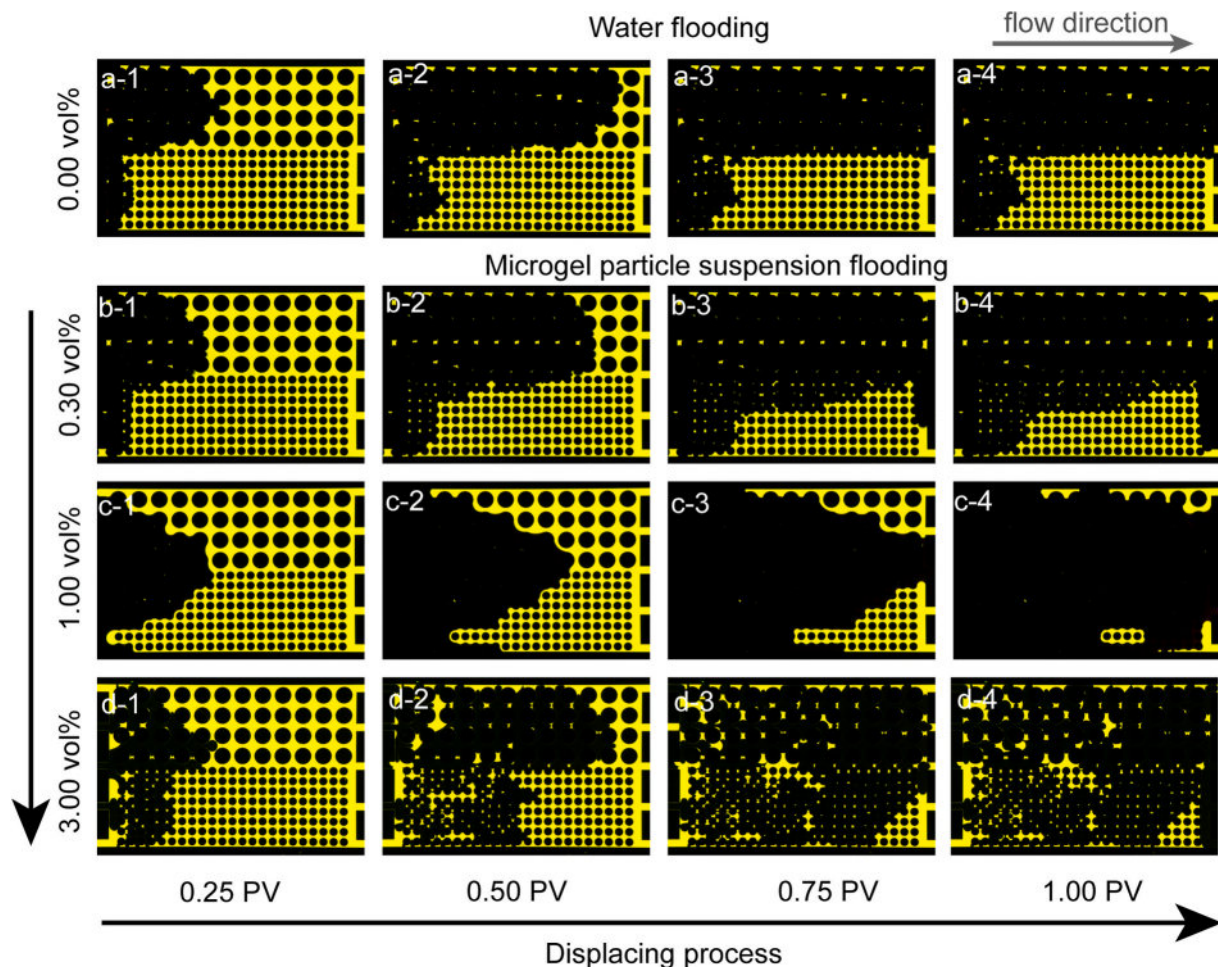


**Fig. 3.** Microfluidic experimental results of multiphase distributions during (a) water flooding and microgel particle suspension flooding at (b) a low injection concentration of 0.30 vol%, (c) an intermediate injection concentration of 1.00 vol%, and (d) a high injection concentration of 3.00 vol% during displacement processes at different representative stages of 0.25 PV, 0.50 PV, 0.75 PV, and 1.00 PV. Yellow is the defending fluid (oil), and black is the solid structures and invading phase. (For interpretation of the references to color in this figure legend, the reader is referred to the Web version of this article.)

## 4. Results and mechanism analysis

### 4.1. Impact of injection particle concentration on displacement patterns

A series of displacement experiments have been performed on micromodels with bipermeability structures by varying the injection particle concentration. These processes of microgel particle suspension flooding (Fig. 3b, c, 3d) were compared with those of deionized water flooding (Fig. 3a). During deionized water flooding, the preferential flow path quickly formed in the high permeable layer, leaving most residual oil trapped in the lower permeable layer (Fig. 3a). Although the microgel particle size was much smaller than the smallest pore size in the micromodels, it was surprisingly found that such preferential flow can be suppressed by microgel particle suspension flooding, and their ability depends on the injection particle concentration, as shown in Fig. 3 b, 3c, 3 d. Similar to the poorest profile of water flooding, microgel particle suspension flooding at the low injection concentration (0.30 vol %) also presented obvious fluid channeling phenomena in which an increasing number of invading phases converged into the highly permeable layer (Fig. 3b). At the intermediate injection concentration, a stable synchronous displacement process was realized in both layers as a displacement process in a homogeneous porous medium. At high injection concentrations, the fluctuation transport mode became obvious, and the preferential flow pathway changed frequently. Three different transport modes were identified: (1) the channeling mode at the low injection concentration (0.30 vol%), (2) the synchronous mode at an intermediate injection concentration (1.00 vol%), and (3) the fluctuation mode at the high injection concentration (3.00 vol%).

Pore-scale numerical simulations were performed to discover the physics of the observed different transport modes. Fig. 4 shows the corresponding simulated invasion morphologies. They were generally

consistent with the experimental results at low and intermediate injection concentrations, but the fluctuation transport behaviors at high concentrations (Fig. 3d) cannot be described by the current simulation model (Fig. 4d). Inspection of the particle concentration distributions (Fig. 4b and c) shows that nonuniform particle concentration exists in different layers, which may play an essential role in preferential flow control at low and intermediate concentrations, compared with no particle concentration manipulation effect in water flooding (Fig. 4a), but merely advection-diffusion induced concentration difference in our current simulation was not enough for fluctuation phenomena at high injection concentration (Fig. 4d).

Furthermore, the invading process and the invading phase saturation difference between the higher and lower permeable layers at different stages were obtained to evaluate the preferential flow suppression ability quantitatively in both experiments and simulations, as shown in Fig. 5. From Fig. 5a, it can be observed that the transport modes in heterogeneous porous media can be generally reproduced by simulation in the case of low and intermediate injection concentrations but cannot be reproduced at high injection concentrations. Except for the strange result of a high injection concentration, the simulation results show that a higher injection concentration can promote increasing fluid flow through the low-permeability layer. The preferential flow suppression ability of low and intermediate injection concentrations can be described well by the current simulation model, as shown in Fig. 5b and c. The intermediate injection concentration can always maintain the lowest saturation difference and obtain the optimal preferential suppression effect during the displacement process. In Fig. 5b, the invading phase saturation difference curve in the experiments shows fluctuations at high injection particle concentrations, which can also be observed in Fig. 5a.

However, the simulation results at high injection particle

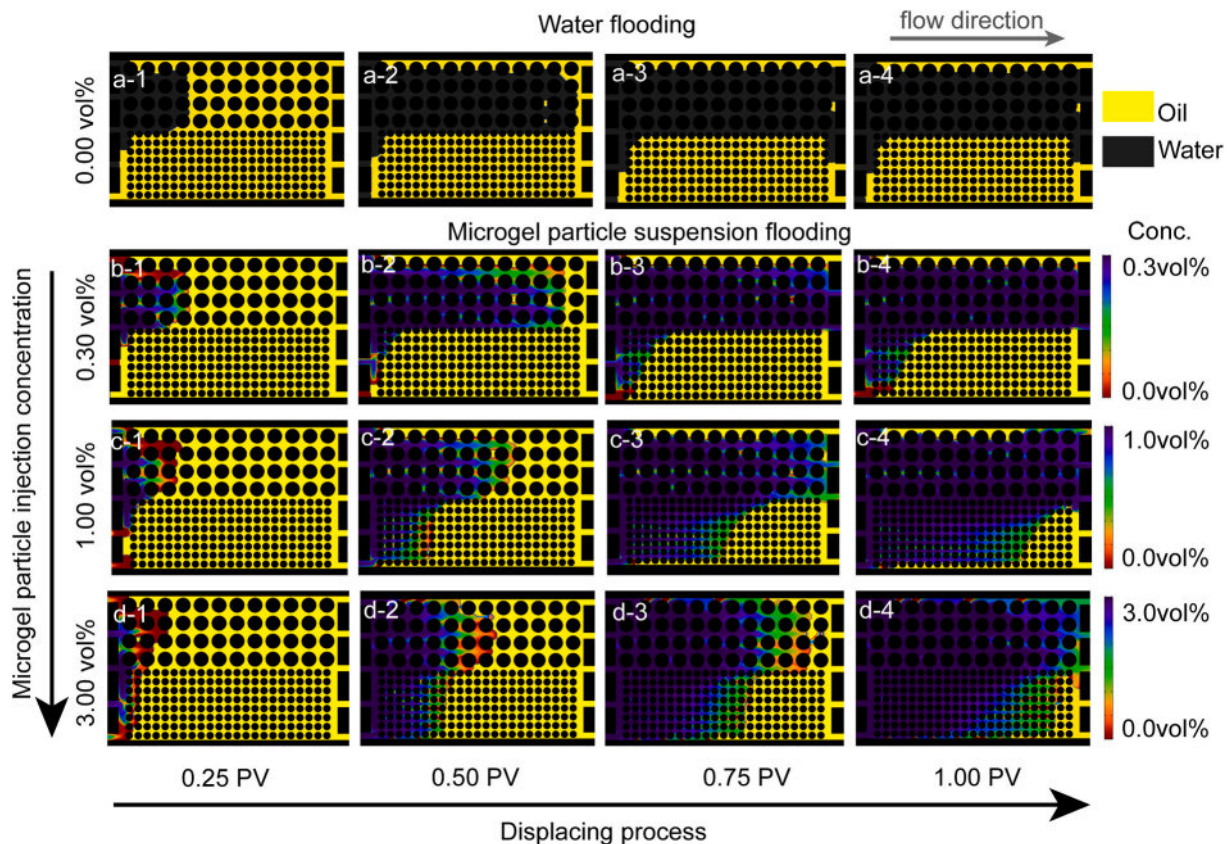


Fig. 4. Numerical simulation results of multiphase distributions during (a) water flooding and microgel particle suspension flooding with (b) a low concentration of 0.30 vol%, (c) an intermediate concentration of 1.00 vol%, and (d) a high concentration of 3.00 vol% in displacement processes at different representative stages of 0.25 PV, 0.50 PV, 0.75 PV, and 1.00 PV.

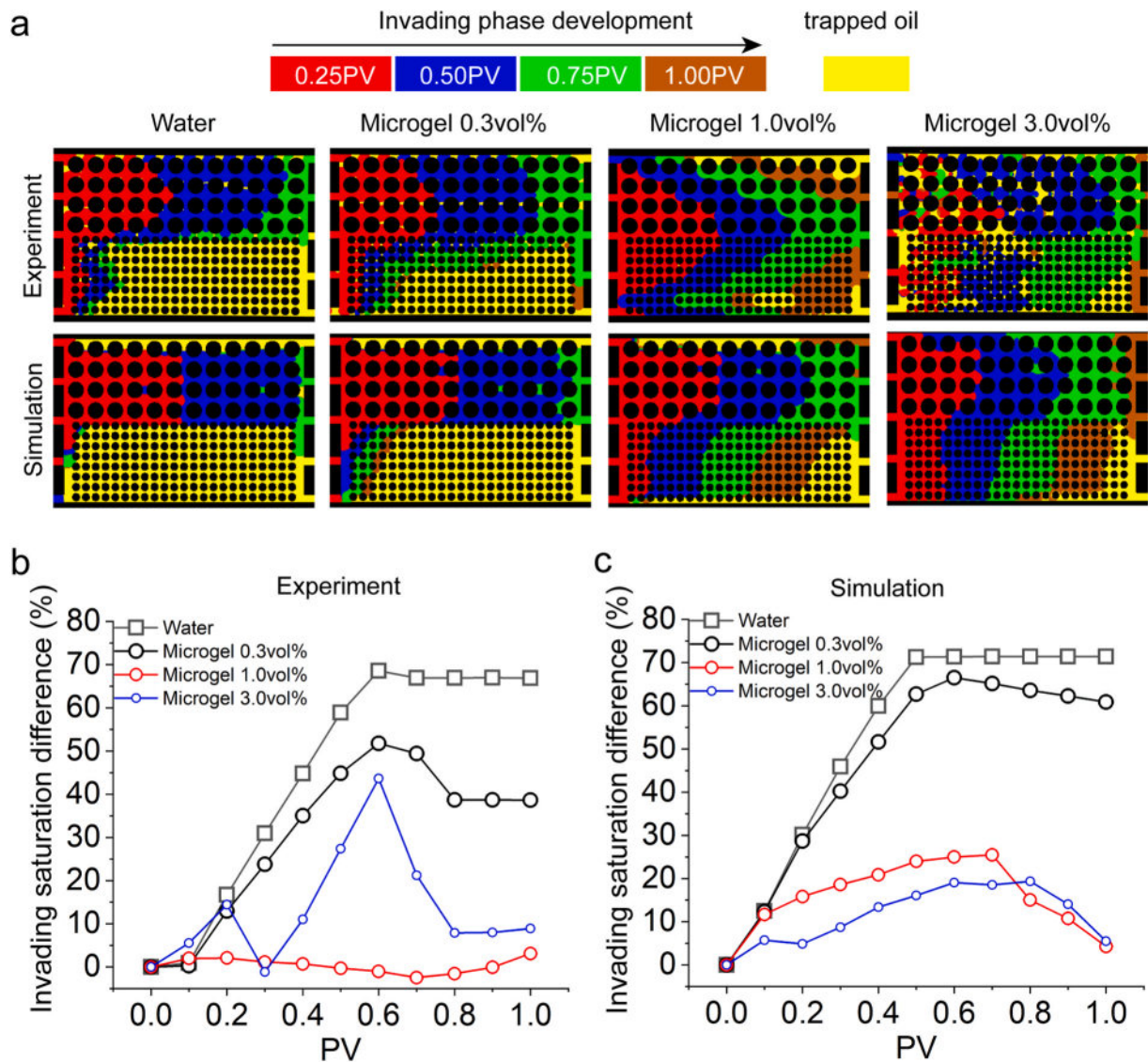


Fig. 5. (a) The invading phase development in experiments and simulations. (b) Experimental and (c) simulation results of the evolution of the defending phase saturation differences between the higher and lower permeable layers.

concentrations still present a stable process without the upward or downward shifts in Fig. 5c. The discrepancy at high injection concentrations may be attributed to underlying particle transport physics, which were not considered in the current simulation model. The advection-diffusion equation governs the particle transport process in the current simulation model but cannot reflect particle inertia, fluid-particle relative drift velocity, and the impact of particles on fluid flow, which may not be ignored at high injection concentrations, especially for larger particles. Further study is required to eliminate the discrepancy between experiments and simulations and clarify the potential mechanism of fluctuations.

#### 4.2. Pore-scale observation and mechanism analysis

Microfluidic observations and simulations directly determine the different macroscopic patterns, but they also left some confusion about how concentration manipulates invading flow pathways at low and intermediate injection concentrations and why the current numerical model was no longer applicable at high injection concentrations. By coloring all the particles with fluorescence and a relatively long exposure time at the local view, it can be observed the particle concentration

distribution in the different positions of the micromodel, as shown in Fig. 6. It was obvious that the concentration of the higher permeable layer was significantly higher than that of the lower permeable layer at low and intermediate injection concentrations, as shown in Fig. 6a and b, respectively. However, at high injection concentrations, the concentration field was quite complicated and changes over time, as shown in Fig. 6c. The concentration field in porous media presents the strong concentration-adjusted feature that the hysteresis of the particles will cause a drastic particle concentration increase in the preferential flow pathway and then divert the following fluid into the low permeable layer. The displacing fronts in the higher and lower permeable parts move forward alternately, and the lower permeable front can even be ahead of the higher permeable front at 0.33 PV (Fig. 6c). Compared with the relatively stable and continuous particle concentration distribution at low and intermediate injection concentrations, the particle transport behaviors at high injection concentrations present an unstable displacement process with sensitive particle concentration changes and local particle rapid enrichment by particles lagging behind the displacing fluid, which explains the invalidation of our current numerical model.

Something inspiring can be found from quantitative comparisons of

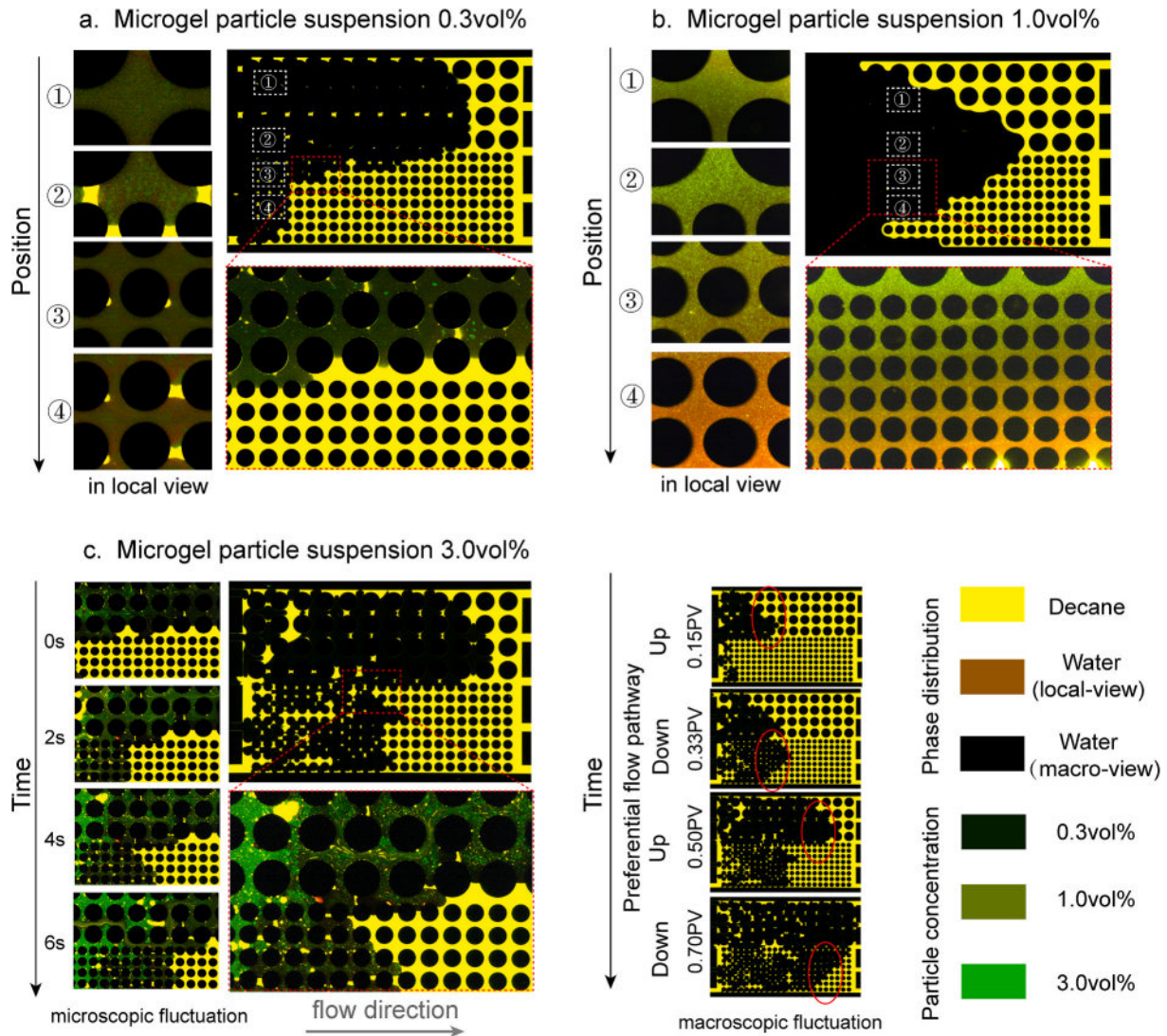


**Fig. 6.** Microgel particle distribution of (a) low concentration 0.3 vol%, and larger red box shows the flow channelling formation at the interface of higher and lower permeable layer, (b) intermediate concentration 0.3 vol%, and larger red box shows concentration distribution from higher permeable layer to lower permeable layer. The local view from positions 1–4 shows different particle concentrations, and the emission light of fluorescent microgel particles is green. (c) The strong fluctuation flow field and complex microgel particle distribution at a high concentration of 3.0 vol%. (For interpretation of the references to color in this figure legend, the reader is referred to the Web version of this article.)

the particle concentration distribution between the microfluidic experiments and the numerical simulation results at low and intermediate concentrations (Fig. 7). In this study, the straight line near the displacement front of the low permeability channel was selected as the standard comparison line. When the injected particle concentration was intermediate or low, the concentration distribution of the experiment and the numerical simulation were in good agreement, which further demonstrates that these transport processes follow the model of non-Newtonian two-phase flow with particle advection-diffusion in the invading phase. Since the viscosity sensitivity of the concentration at the low concentration point was much smaller than that at the intermediate concentration point ( $Rs = \frac{\partial \eta / \partial c|_{c=0.3\text{vol}\%}}{\partial \eta / \partial c|_{c=1.0\text{vol}\%}} = 0.24$ ,  $Rs$  is the ratio of viscosity sensitivity to concentration) and the concentration difference range of the low injection concentration was small, the low injection concentration was too weak to change the preferential flow pathway, while the intermediate concentration can indeed spontaneously adjust the concentration between the higher and lower permeable layers to self-adapt the flow field in the heterogeneous structure.

The adjustment of the velocity field in heterogeneous porous media

with low and intermediate injection particle concentrations of microgel particle suspensions are compared in Fig. 8. Comparing Fig. 8 a1 and b1, it can be observed that the intermediate injection particle concentration can significantly weaken the velocity of the high permeability layer and increase the velocity of the low permeability layer. Although a large amount of fluid enters the higher permeable layer at the inlet, the lower permeable layer at the outlet exhibits a higher velocity, which means that effective concentration manipulation can redistribute the flow field in heterogeneous porous media (see Fig. 8 b1). Comparing the flow direction of low and intermediate injection concentrations by extracting snapshots of the streamlines, as shown in Fig. 8 a2 and b2, a large number of vertical streamlines were discovered at intermediate injection concentrations, which diverted the invading fluid from the higher permeable layer to the lower permeable layer (Fig. 8 b2). An enlarged view of two streamline snapshots presents more details of the diversion streamlines near the fluid-fluid interface at low and intermediate injection particle concentrations, as shown in Fig. 8 a3 and b3, respectively.

In summary, the results of microfluidic experiments and numerical simulations at low and intermediate concentrations are consistent and

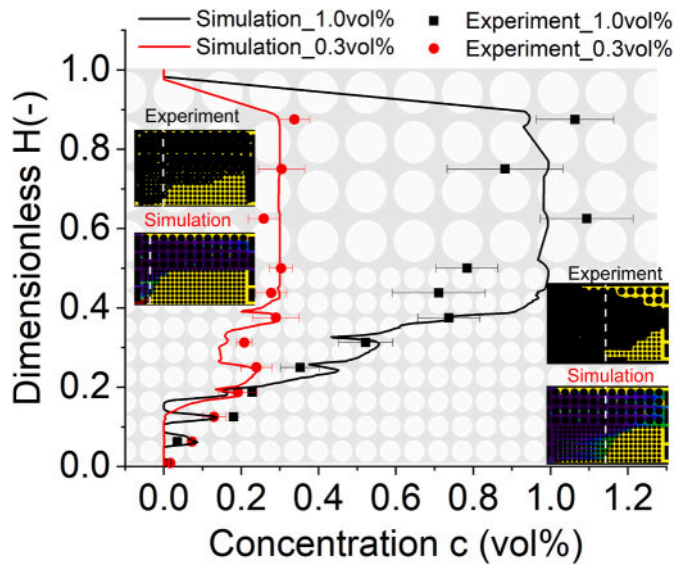


Fig. 7. The contrast of the concentration distribution at the displacement front between the numerical simulation and microfluidic experiment. The concentration distribution curve of the numerical simulation is selected at the cross-section of the displacement front at 0.75 PV (the position of the white dashed line in the small picture). The experimental data are the average concentration distribution of each pore in the displacement front at the breakthrough time.

prove that different concentrations do appear in the high-permeability layer and the low-permeability layer, and self-adjustment can be realized in heterogeneous porous media. This process was dominated by the current simulation model of non-Newtonian two-phase flow with

particle advection-diffusion in the invading phase. However, it is worth noting that the fluctuation displacement mode at high injection concentrations shows that strong particle hysteresis-induced excessive self-adaptivity can alternate the preferential flow pathway frequently, and the current numerical simulation model was invalid to describe such unstable flow.

However, it should be noted that these transport mechanisms presented here were from idealized heterogeneous porous media (dual-permeability model), so modifications should be introduced when the statistical distribution of heterogeneity in microstructures and hydraulic properties occurs. In addition, the plugging effect may not be ignored in natural porous media; if there are a significant number of microgel particles comparable to or larger than the pore size, this flow control effect by concentration-manipulated rheology of the microgel particle suspension should be combined with the plugging effect. All those problems should be analyzed in future work. Regardless, the results clearly demonstrate the major role of concentration-manipulated rheology and a nonuniform particle concentration distribution when the particle size effect is negligible. The outcomes and comprehensive understandings from this study can direct more effective microgel particle suspension applications for enhanced oil recovery and may also lead to novel designs for microgel particle suspensions.

### 5. Conclusions

This study presents a novel preferential flow suppression effect by microgel particle suspension when the particle size is much smaller than the pore size. Concentration-manipulated rheology of microgel particle suspensions is a prerequisite for particle concentration control of the flow field. By varying the microgel particle suspension concentration, three transport modes are investigated via microfluidic experiments: (1) the channeling mode at low concentrations, (2) the optimal synchronous

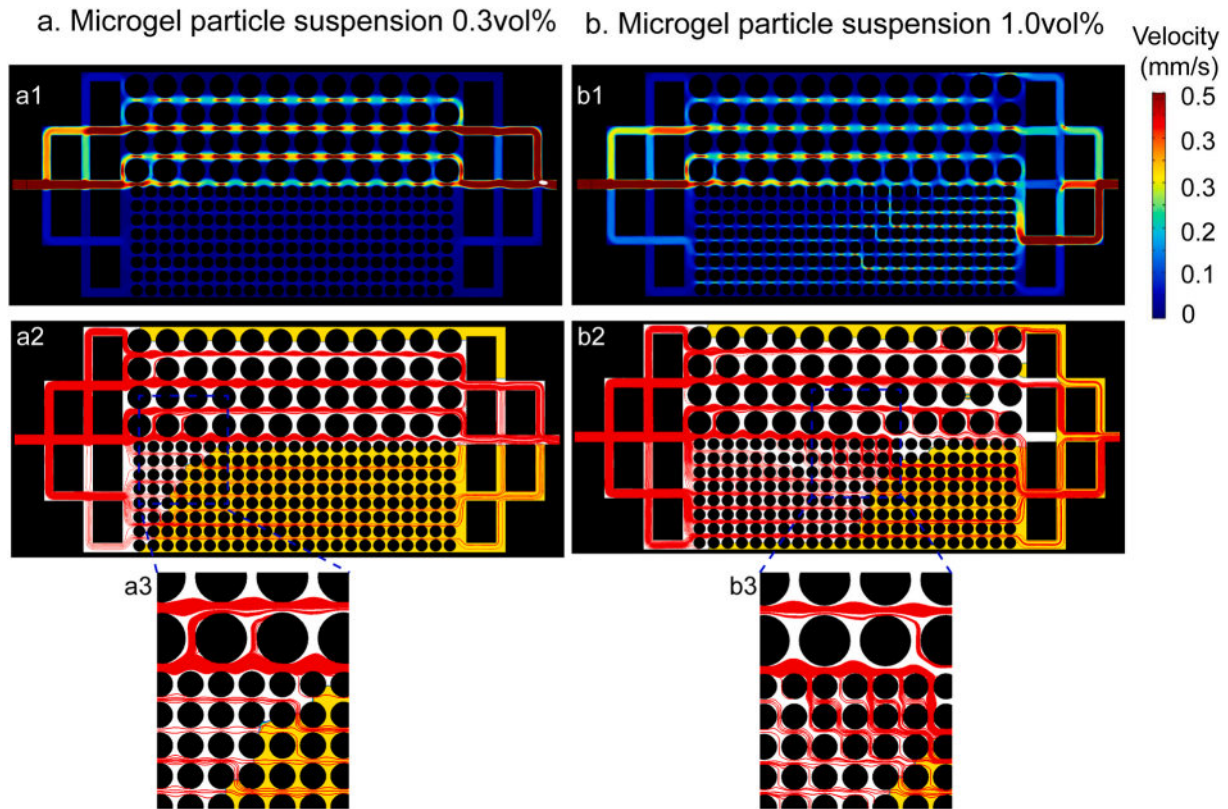


Fig. 8. Comparisons of velocity distribution (a1, b1) and streamlines (a2, b2) extracted from snapshots of numerical simulation results at 0.75 PV during microgel particle suspension flooding with (a1, a2, a3) a low injection concentration of 0.30 vol% and (b1, b2, b3) an intermediate injection concentration of 1.00 vol%, (a3, b3) local enlarged streamlines. They were used to present the diversion phenomena from the higher permeable layer to the lower permeable layer.

mode at intermediate concentrations, and (3) the fluctuation mode induced by high concentrations. By the combination of experimental and numerical analysis, it was found that the transport behaviors at low and intermediate concentrations can be described by our current model - non-Newtonian two-phase flow with particle advection-diffusion in the aqueous phase, while the strong particle retention phenomenon at high concentration cannot be realized by our current model. The results of the low and intermediate injection concentrations proved that a nonuniform concentration distribution does appear in the different layers, but the self-adaptation ability of microgel particle suspensions is controlled by their injection concentration. The intermediate concentration can realize uniform flow in heterogeneous porous media by moderately diverting the water from the high permeable layer to the low permeable layer, while the low concentration is too weak to overcome the preferential flow. The high injection concentration is too excessive and causes a preferential flow pathway to alternate frequently, which may trap many oil ganglia in the porous media.

#### Author credit statement

**Wenhai Lei:** Investigation, Software, Validation, Writing Original draft preparation. **Qiangqiang Li:** Investigation. **Hai-En Yang:** Data Curation. **Tian-Jiang Wu:** Resources. **Jiong Wei:** Software. **Moran Wang:** Conceptualization, Supervision, Writing- Reviewing and Editing, Project administration.

#### Declaration of competing interest

The authors declare that they have no known competing financial interests or personal relationships that could have appeared to influence the work reported in this paper.

#### Acknowledgments

This work is financially supported by the National Key Research and Development Program of China (No. 2019YFA0708704) and the NSF grant of China (No. U1837602). We would like to sincerely acknowledge Dr. Mengquan Shi from the Technical Institute of Physics and Chemistry, Chinese Academy of Sciences, for his help with microgel particle synthesis.

#### References

Abdulbaki, M., Huh, C., Sepehrmoori, K., Delshad, M., Varavei, A., 2014. A critical review on use of polymer microgels for conformance control purposes. *J. Petrol. Sci. Eng.* 122, 741–753.

Abrams, A., 1977. Mud design to minimize rock impairment due to particle invasion. *J. Petrol. Technol.* 29 (5), 586–592.

Arshadi, M., Khishvand, M., Aghaei, A., Piri, M., Al-Muntasheri, G.A., 2018. Pore-scale experimental investigation of two-phase flow through fractured porous media. *Water Resour. Res.* 54 (5), 3602–3631.

Bai, B., Liu, Y., Coste, J.-P., Li, L., 2007. Preformed particle gel for conformance control: transport mechanism through porous media. *SPE Reservoir Eval. Eng.* 10 (2), 176–184.

Barkman, J.H., Davidson, D.H., 1972. Measuring water quality and predicting well impairment. *J. Petrol. Technol.* 24 (7), 865–873.

Blunt, M.J., 2017. *Multiphase Flow in Permeable Media: A Pore-Scale Perspective*. Cambridge University Press, Cambridge.

Browne, C.A., Shih, A., Datta, S.S., 2020. Pore-scale flow characterization of polymer solutions in microfluidic porous media. *Small* 16 (9), 1903944.

Cahn, J.W., 1959. Free energy of a nonuniform system. II. Thermodynamic basis. *J. Chem. Phys.* 30 (5), 1121–1124.

Cahn, J.W., Hilliard, J.E., 1958. Free energy of a nonuniform system. I. Interfacial free energy. *J. Chem. Phys.* 28 (2), 258–267.

Cahn, J.W., Hilliard, J.E., 1959. Free energy of a nonuniform system. III. Nucleation in a two-component incompressible fluid. *J. Chem. Phys.* 31 (3), 688–699.

Chen, X., et al., 2020. Core- and pore-scale investigation on the migration and plugging of polymer microspheres in a heterogeneous porous media. *J. Petrol. Sci. Eng.* 195, 107636.

Chomsurin, C., Werth, C.J., 2003. Analysis of pore-scale nonaqueous phase liquid dissolution in etched silicon pore networks. *Water Resour. Res.* 39 (9), 1265.

Cieplak, M., Robbins, M.O., 1988. Dynamical transition in quasistatic fluid invasion in porous media. *Phys. Rev. Lett.* 60 (20), 2042–2045.

Cieplak, M., Robbins, M.O., 1990. Influence of contact angle on quasistatic fluid invasion of porous media. *Phys. Rev. B* 41 (16), 11508–11521.

Conn, C.A., Ma, K., Hirasaki, G.J., Biswal, S.L., 2014. Visualizing oil displacement with foam in a microfluidic device with permeability contrast. *Lab Chip* 14 (20), 3968–3977.

Cueto-Felgueroso, L., Juanes, R., 2008. Nonlocal interface dynamics and pattern formation in gravity-driven unsaturated flow through porous media. *Phys. Rev. Lett.* 101 (24), 244504.

Dai, C., et al., 2017. Investigation on matching relationship between dispersed particle gel (DPG) and reservoir pore-throats for in-depth profile control. *Fuel* 207, 109–120.

Datta, S.S., Ramakrishnan, T.S., Weitz, D.A., 2014. Mobilization of a trapped non-wetting fluid from a three-dimensional porous medium. *Phys. Fluids* 26 (2), 022002.

Ferrari, A., Jimenez-Martinez, J., Borgne, T.L., Méheust, Y., Lunati, L., 2015. Challenges in modeling unstable two-phase flow experiments in porous micromodels. *Water Resour. Res.* 51 (3), 1381–1400.

Gong, Y., Wang, M., Zhang, Z., He, J., 2018. Microgel evolution at three-phase contact region and associated wettability alteration. *Colloids Surf. A Physicochem. Eng. Asp.* 558, 297–302.

Gong, Y., Zhang, Z., He, J., 2017. Deformation and stability of core-shell microgels at oil/water interface. *Ind. Eng. Chem. Res.* 56 (50), 14793–14798.

Grate, J.W., et al., 2013. Silane modification of glass and silica surfaces to obtain equally oil-wet surfaces in glass-covered silicon micromodel applications. *Water Resour. Res.* 49 (8), 4724–4729.

Gu, Q., Liu, H., Wu, L., 2021. Preferential imbibition in a dual-permeability pore network. *J. Fluid Mech.* 915, A138.

Holtzman, R., Segre, E., 2015. Wettability stabilizes fluid invasion into porous media via nonlocal, cooperative pore filling. *Phys. Rev. Lett.* 115 (16), 164501.

Hu, R., Lan, T., Wei, G.-J., Chen, Y.-F., 2019. Phase diagram of quasi-static immiscible displacement in disordered porous media. *J. Fluid Mech.* 875, 448–475.

Huppert, H.E., Neufeld, J.A., 2014. The fluid mechanics of carbon dioxide sequestration. *Annu. Rev. Fluid Mech.* 46 (1), 255–272.

Imqam, A., Bai, B., Delshad, M., 2018. Micro-particle gel transport performance through unconsolidated sandstone and its blocking to water flow during conformance control treatments. *Fuel* 231, 479–488.

Khan, M.R., et al., 2016. Megacity pumping and preferential flow threaten groundwater quality. *Nat. Commun.* 7 (1), 12833.

Lai, C.-Y., et al., 2018. Foam-driven fracture. *Proc. Natl. Acad. Sci. U. S. A.* 115 (32), 8082.

Le Goc, R., de Dreuzy, J.R., Davy, P., 2010. Statistical characteristics of flow as indicators of channeling in heterogeneous porous and fractured media. *Adv. Water Resour.* 33 (3), 257–269.

Lei, W., et al., 2020. Enhanced oil recovery mechanism and recovery performance of micro-gel particle suspensions by microfluidic experiments. *Energy Sci. Eng.* 8 (4), 986–998.

Lei, W., Xie, C., Wu, T., Wu, X., Wang, M., 2019. Transport mechanism of deformable micro-gel particle through micropores with mechanical properties characterized by AFM. *Sci. Rep.* 9 (1), 1453.

Lenormand, R., Zarcone, C., Sarr, A., 1983. Mechanisms of the displacement of one fluid by another in a network of capillary ducts. *J. Fluid Mech.* 135 (135), 337–353.

Lenhof, A., Laurrell, T., 2010. Continuous separation of cells and particles in microfluidic systems. *Chem. Soc. Rev.* 39 (3), 1203–1217.

Levaché, B., Bartolo, D., 2014. Revisiting the saffman-taylor experiment: imbibition patterns and liquid-entrainment transitions. *Phys. Rev. Lett.* 113 (4), 044501.

Li, S., et al., 2020. Understanding transport of an elastic, spherical particle through a confining channel. *Appl. Phys. Lett.* 116 (10), 103705.

Liu, Y., et al., 2019. Novel chemical flooding system based on dispersed particle gel coupling in-depth profile control and high efficient oil displacement. *Energy Fuels* 33 (4), 3123–3132.

Ma, K., Liontas, R., Conn, C.A., Hirasaki, G.J., Biswal, S.L., 2012. Visualization of improved sweep with foam in heterogeneous porous media using microfluidics. *Soft Matter* 8 (41), 10669.

Monteillet, H., et al., 2014. Ultrastrong anchoring yet barrier-free adsorption of composite microgels at liquid interfaces. *Adv. Mater. Interfac.* 1 (7), 1300121.

Moreno, L., Tsang, C.-F., 1994. Flow channeling in strongly heterogeneous porous media: a numerical study. *Water Resour. Res.* 30 (5), 1421–1430.

Pritchett, J., et al., 2003. Field application of a new in-depth waterflood conformance improvement tool. In: *SPE International Improved Oil Recovery Conference in Asia Pacific*. Society of Petroleum Engineers, Kuala Lumpur, Malaysia.

Rabbani, H.S., et al., 2018. Suppressing viscous fingering in structured porous media. *Proc. Natl. Acad. Sci. U. S. A.* 115 (19), 4833.

Sackmann, E.K., Fulton, A.L., Beebe, D.J., 2014. The present and future role of microfluidics in biomedical research. *Nature* 507 (7491), 181–189.

Shahnazari, M.R., Maleka Ashtiani, I., Saberi, A., 2018. Linear stability analysis and nonlinear simulation of the channeling effect on viscous fingering instability in miscible displacement. *Phys. Fluids* 30 (3), 034106.

Shokri, H., Kayhani, M.H., Norouzi, M., 2017. Nonlinear simulation and linear stability analysis of viscous fingering instability of viscoelastic liquids. *Phys. Fluids* 29 (3), 033101.

Siena, M., Iliev, O., Prill, T., Riva, M., Guadagnini, A., 2019. Identification of channeling in pore-scale flows. *Geophys. Res. Lett.* 46 (6), 3270–3278.

Smith, J.E., Liu, H., Guo, Z.D., 2000. Laboratory studies of in-depth colloidal dispersion gel Technology for daqing oil field. In: *SPE/AAPG Western Regional Meeting*. Society of Petroleum Engineers, Long Beach, California, p. 13.

Style, R.W., Isa, L., Dufresne, E.R., 2015. Adsorption of soft particles at fluid interfaces. *Soft Matter* 11 (37), 7412–7419.

- Suo, S., Liu, M., Gan, Y., 2020. Fingering patterns in hierarchical porous media. *Phys. Rev. Fluids* 5 (3), 034301.
- Tan, C.T., Homsy, G.M., 1988. Simulation of nonlinear viscous fingering in miscible displacement. *Phys. Fluids* 31 (6), 1330–1338.
- Wang, C., Mehmani, Y., Xu, K., 2021. Capillary equilibrium of bubbles in porous media. *Proc. Natl. Acad. Sci. U. S. A* 118 (17), e2024069118.
- Wang, Z., Chauhan, K., Pereira, J.-M., Gan, Y., 2019. Disorder characterization of porous media and its effect on fluid displacement. *Phys. Rev. Fluids* 4 (3), 034305.
- Watanabe, N., Hirano, N., Tsuchiya, N., 2009. Diversity of channeling flow in heterogeneous aperture distribution inferred from integrated experimental-numerical analysis on flow through shear fracture in granite. *J. Geophys. Res. Solid Earth* 114, B04208.
- Xie, C., Lei, W., Balhoff, M.T., Wang, M., Chen, S., 2021. Self-adaptive preferential flow control using displacing fluid with dispersed polymers in heterogeneous porous media. *J. Fluid Mech.* 906, A10.
- Xie, C., Lv, W., Wang, M., 2018. Shear-thinning or shear-thickening fluid for better EOR?—A direct pore-scale study. *J. Petrol. Sci. Eng.* 161, 683–691.
- Xie, C., Xu, K., Mohanty, K., Wang, M., Balhoff, M.T., 2020. Nonwetting droplet oscillation and displacement by viscoelastic fluids. *Phys. Rev. Fluids* 5 (6), 063301.
- Xie, C., Zhang, J., Bertola, V., Wang, M., 2016. Lattice Boltzmann modeling for multiphase viscoplastic fluid flow. *J. Non-Newtonian Fluid Mech.* 234, 118–128.
- Yamada, M., Seki, M., 2005. Hydrodynamic filtration for on-chip particle concentration and classification utilizing microfluidics. *Lab Chip* 5 (11), 1233–1239.
- Yao, C., Lei, G., Cathles, L.M., Steenhuis, T.S., 2014. Pore-scale investigation of micron-size polyacrylamide elastic microspheres (MPEMs) transport and retention in saturated porous media. *Environ. Sci. Technol.* 48 (9), 5329–5335.
- Yao, C., Lei, G., Gao, X., Li, L., 2013. Controllable preparation, rheology, and plugging property of micron-grade polyacrylamide microspheres as a novel profile control and flooding agent. *J. Appl. Polym. Sci.* 130 (2), 1124–1130.
- Yuan, C., et al., 2019. Deformable Micro-gel for EOR in High-Temperature and Ultra-high-salinity Reservoirs: How to Design the Particle Size of Micro-gel to Achieve its Optimal Match with Pore Throat of Porous Media. Abu Dhabi International Petroleum Exhibition & Conference, Abu Dhabi, UAE.
- Yuan, Q., Zhou, X., Zeng, F., Knorr, K.D., Imran, M., 2018. Investigation of concentration-dependent diffusion on frontal instabilities and mass transfer in homogeneous porous media. *Can. J. Chem. Eng.* 96 (1), 323–338.
- Yue, P., Feng, J.J., Liu, C., Shen, J.I.E., 2004. A diffuse-interface method for simulating two-phase flows of complex fluids. *J. Fluid Mech.* 515, 293–317.
- Yue, P., Zhou, C., Feng, J.J., Ollivier-Gooch, C.F., Hu, H.H., 2006. Phase-field simulations of interfacial dynamics in viscoelastic fluids using finite elements with adaptive meshing. *J. Comput. Phys.* 219 (1), 47–67.
- Zhang, H., Bai, B., 2011. Preformed-particle-Gel transport through open fractures and its effect on water flow. *SPE J.* 16 (2), 388–400.
- Zhao, B., MacMinn, C.W., Juanes, R., 2016. Wettability control on multiphase flow in patterned microfluidics. *Proc. Natl. Acad. Sci. U. S. A* 113 (37), 10251–10256.
- Zhao, G., et al., 2018. Preparation and application of a novel phenolic resin dispersed particle gel for in-depth profile control in low permeability reservoirs. *J. Petrol. Sci. Eng.* 161, 703–714.
- Zhao, H., et al., 2013. Study on plugging performance of cross-linked polymer microspheres with reservoir pores. *J. Petrol. Sci. Eng.* 105, 70–75.